MITSUBISHI ELECTRIC RESEARCH LABORATORIES
http://www.merl.com

Station-keeping and momentum-management on halo orbits around L2: Linear-quadratic feedback and model predictive control approaches

Kalabić, U.; Weiss, A.; Di Cairano, S.; Kolmanovsky, I.V.

TR2015-002 January 11, 2015

Abstract

The control of station-keeping and momentum-management is considered while tracking a halo orbit centered at the second Earth-Moon Lagrangian point. Multiple schemes based on linear-quadratic feedback control and model predictive control (MPC) are considered and it is shown that the method based on periodic MPC performs best for position tracking. The scheme is then extended to incorporate attitude control requirements and numerical simulations are presented demonstrating that the scheme is able to achieve simultaneous tracking of a halo orbit and dumping of momentum while enforcing tight constraints on pointing error.

AAS/AIAA Space Flight Mechanics Meeting

AAS 15-307

STATION-KEEPING AND MOMENTUM-MANAGEMENT ON HALO ORBITS AROUND L2: LINEAR-QUADRATIC FEEDBACK AND MODEL PREDICTIVE CONTROL APPROACHES

Uroš Kalabić,* Avishai Weiss,† Ilya Kolmanovsky,‡ and Stefano Di Cairano§

The control of station-keeping and momentum-management is considered while tracking a halo orbit centered at the second Earth-Moon Lagrangian point. Multiple schemes based on linear-quadratic feedback control and model predictive control (MPC) are considered and it is shown that the method based on periodic MPC performs best for position tracking. The scheme is then extended to incorporate attitude control requirements and numerical simulations are presented demonstrating that the scheme is able to achieve simultaneous tracking of a halo orbit and dumping of momentum while enforcing tight constraints on pointing error.

INTRODUCTION

The paper considers the control of a spacecraft near the second Lagrangian point L2 in the Earth-Moon orbital system. The objective is to determine an appropriate method for the stabilization of a spacecraft to a halo orbit while simultaneously stabilizing the attitude of the spacecraft to stay inertially fixed.

Halo orbits are unstable limit cycles centered around the collinear Lagrangian points that are unforced solutions to the restricted 3-body problem. The halo orbit about L2 is particularly interesting because L2 is behind the Moon and because it is the point with the lowest gravitational potential energy needed to escape the Earth-Moon system (see Figure 1); a satellite or space station following a sufficiently large halo orbit trajectory could facilitate communication between Earth and the far side of the Moon and also serve as a launchpad for faraway space missions.

The shape of a halo orbit is complex and a spacecraft would have complex dynamics when pointing at an object in its vicinity. Because it is difficult and not necessary to point at a nearby object such as the Earth or Moon, we instead consider the stabilization of the attitude so that the spacecraft point at a distant star and thereby remain almost inertially fixed.

A halo orbit trajectory coupled with an inertially fixed orientation are unforced solutions to the idealized and decoupled translational and attitude equations of motion governing the spacecraft. Using these, we are able to develop control schemes that stabilize these trajectories such that fuel is consumed only when correcting tracking and attitude errors. In addition to asymptotically stabilizing the error, the schemes under consideration are required to enforce system constraints; these

*Graduate Student, Aerospace Engineering, University of Michigan, 1320 Beal Avenue, Ann Arbor, MI 48109.
†Member Research Staff, Mechatronics, MERL, 201 Broadway, Cambridge, MA 02139.
‡Professor, Aerospace Engineering, University of Michigan, 1320 Beal Avenue, Ann Arbor, MI 48109.
§Senior Principal Member Research Staff, Mechatronics, MERL, 201 Broadway, Cambridge, MA 02139.

constraints can include limits on the available thrust as well as constraints on pointing error. Furthermore, the constraints considered in this paper serve to couple the translational and attitude dynamics because the constrained thrusters need to simultaneously stabilize the tracking and attitude errors. In order to satisfy the above, in the following we propose discrete-time trajectory-tracking control schemes that are based on linear-quadratic (LQ) and model predictive control (MPC) methods.

The schemes are based on the linearized discretization of the tracking error dynamics. These dynamics are linear but time-varying and schemes are considered based on averaged, instantaneously fixed, and periodic dynamics. The schemes are tested in a nonlinear simulation of the Earth-Moon system and the scheme based on periodic MPC applied to dynamics discretized using one hour time-steps is shown to perform best while adhering to constraints on available computational power.

The simulations show that MPC can be used to simultaneously guarantee trajectory-tracking while controlling the attitude and enforcing constraints. Furthermore, a more realistic simulation is provided for the case where the orbit between the primaries has non-zero eccentricity.

The paper is organized as follows. The rest of the introduction describes the problem formulation. The next section presents three LQ control schemes and three MPC control schemes. The section after next presents numerical results and the final section is the conclusion.

Station-Keeping on Halo Orbits about L2

Generally in a system of two bodies orbiting around a common barycenter, the Lagrangian (or libration) points are the points at which the gravitational and centrifugal forces cancel out in the orbital frame $\mathcal{F}_O$, which is scaled so that the distance between the two bodies remains constant. See Reference 1 for a more detailed presentation than available here. There are five Lagrangian points, labeled L1 through L5; the first three points L1 through L3 are called collinear because they lie on the x-axis. The other two are called triangular. A contour plot of the rotated gravitational potential energy of the Earth-Moon system is shown in Figure 1 with Lagrangian points labeled.

It is well-known[1,2,3] that the collinear points L1 and L2 are unstable and that there exist unstable orbits about them to which one can stabilize a spacecraft. These orbits are termed halo orbits.[4]

We are concerned with the development of control schemes for tracking halo orbits about Earth-Moon L2 and so we derive the equations of motion of a spacecraft of negligible mass in the frame $\mathcal{F}_O$.

Let the coordinates of such a spacecraft be given by (x, y, z). The units are scaled so that both the distance between the Earth and the Moon and the angular momentum of the Earth-Moon system are fixed at 1. Under these assumptions, the equations of motion of the spacecraft are given by,[5]

$$x'' - 2y' = d(\theta)\left(x - \frac{(1-\rho)(x+\rho)}{r_1^3} - \frac{\rho(x-1+\rho)}{r_2^3}\right) + u_x, \tag{1a}$$

$$y'' + 2x' = d(\theta)\left(y - \frac{(1-\rho)y}{r_1^3} - \frac{\rho y}{r_2^3}\right) + u_y, \tag{1b}$$

$$z'' + z = d(\theta)\left(z - \frac{(1-\rho)z}{r_1^3} - \frac{\rho z}{r_2^3}\right) + u_z, \tag{1c}$$

where $d(\theta) = \frac{1}{1+e\cos\theta}$, ρ is the mass ratio of the Earth-Moon system, e is the eccentricity of the orbit, the true anomaly θ is the independent variable, and a prime $'$ denotes differentiation by θ, *i.e.* $\frac{d}{d\theta}$. The variables r_1 and r_2 denote, respectively, the spacecraft's normalized distances from the

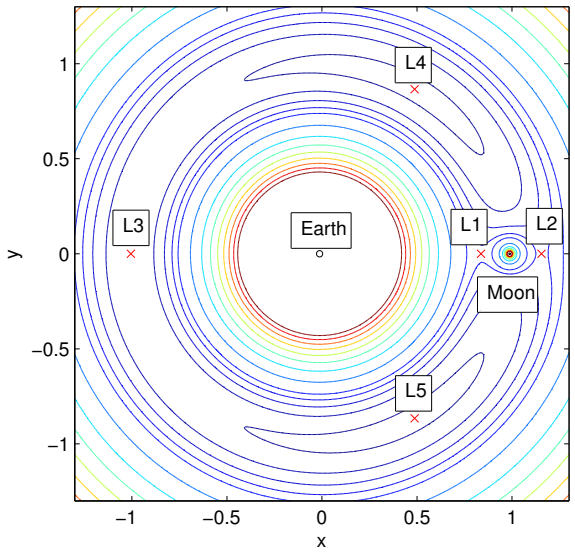

Figure 1. Plot of energy levels in the orbital frame of the Earth-Moon system where $\times$ indicate Lagrangian points

Earth and Moon and satisfy $r_1^2 = (x+\rho)^2 + y^2 + z^2$ and $r_2^2 = (x-1+\rho)^2 + y^2 + z^2$. The variable $\mathbf{u}_t = (u_x, u_y, u_z)$ denotes the acceleration provided by the spacecraft thrusters. For convenience, we introduce a vector $\boldsymbol{\xi} = (x, y, z)$ to denote the position of the spacecraft in the orbital frame.

A halo orbit is a solution to Eq. (1) and its computation for the case where $e = 0$ is described in detail in Reference 3. The computation of halo orbits for the case where $e > 0$ is presented in Reference 5 and references therein.

Momentum-Management

Denote the inertial reference frame by $\mathcal{F}_I$ and the spacecraft body-fixed frame by $\mathcal{F}_B$. Let $\mathbf{J}$ be the moment of inertia of the spacecraft in $\mathcal{F}_B$. Along with thrust, the spacecraft can use its dual-axis thrusters to create a torque about the principal axes and control the attitude of the spacecraft; it can also use its three reaction wheels to dump the adverse momentum that this maneuver causes. Each wheel is placed on a unique principal axis, whose moments of inertia in the directions of the principal axes are $\alpha_1, \alpha_2, \alpha_3$ for the 1-, 2-, and 3-axes, respectively.

Let $\boldsymbol{\nu}$ be the 3-dimensional vector of rotational velocities of the three wheels so that the i-th component of $\boldsymbol{\nu}$ corresponds to the i-th wheel. Assuming very fast controller dynamics, the rotational velocities are controlled by a vector of applied angular accelerations $\mathbf{u}_\alpha$, so that the equations of motion governing $\boldsymbol{\nu}$ are given by $\dot{\boldsymbol{\nu}} = \mathbf{u}_\alpha$.

Let $\mathbf{u}_\tau$ be the torques generated by the thrusters in $\mathcal{F}_B$. Let $\boldsymbol{\omega}$ be the rotational velocity of $\mathcal{F}_B$ with respect to $\mathcal{F}_I$ in the frame $\mathcal{F}_B$ and define,

$$\mathbf{J}_\alpha = \begin{bmatrix} \alpha_1 & & \\ & \alpha_2 & \\ & & \alpha_3 \end{bmatrix}.$$

Therefore the angular momentum of the spacecraft in $\mathcal{F}_B$ is given by $\mathbf{J}\boldsymbol{\omega} + \mathbf{J}_\alpha \boldsymbol{\nu}$.

Let $\mathbf{h}_B$ be the angular momentum of the spacecraft in $\mathcal{F}_I$ and let $\mathbf{C}_B \in \mathrm{SO}(3)$ be a rotation matrix representing a rotation from $\mathcal{F}_I$ to $\mathcal{F}_B$. We derive the equations of motion by beginning with Newton's second law of rotation,[6]

$$\begin{aligned}
\dot{\mathbf{h}}_B &= \mathbf{C}_B^{\mathrm{T}} \mathbf{u}_\tau, \\
\frac{d}{dt}(\mathbf{C}_B^{\mathrm{T}}(\mathbf{J}\boldsymbol{\omega} + \mathbf{J}_\alpha \boldsymbol{\nu})) &= \mathbf{C}_B^{\mathrm{T}} \mathbf{u}_\tau, \\
\mathbf{C}_B^{\mathrm{T}}(\mathbf{J}\dot{\boldsymbol{\omega}} + \mathbf{J}_\alpha \dot{\boldsymbol{\nu}}) + \mathbf{C}_B^{\mathrm{T}} \boldsymbol{\omega}^\times (\mathbf{J}\boldsymbol{\omega} + \mathbf{J}_\alpha \boldsymbol{\nu}) &= \mathbf{C}_B^{\mathrm{T}} \mathbf{u}_\tau, \\
\mathbf{J}\dot{\boldsymbol{\omega}} + \mathbf{J}_\alpha \mathbf{u}_\alpha + \boldsymbol{\omega}^\times (\mathbf{J}\boldsymbol{\omega} + \mathbf{J}_\alpha \boldsymbol{\nu}) &= \mathbf{u}_\tau. \qquad (2)
\end{aligned}$$

Finally, because in the sequel we are only interested in the local stabilization of the attitude, we introduce a 3-2-1 Euler angle parametrization[2] of $\mathbf{C}_B$ and a vector of Euler angles $\boldsymbol{\phi} = (\phi_1, \phi_2, \phi_3)$ so that the equations of motion governing the attitude dynamics are,

$$\dot{\boldsymbol{\phi}} = \mathbf{S}^{-1} \boldsymbol{\omega}, \qquad (3a)$$

$$\mathbf{J}\dot{\boldsymbol{\omega}} = -\boldsymbol{\omega}^\times (\mathbf{J}\boldsymbol{\omega} + \mathbf{J}_\alpha \boldsymbol{\nu}) - \mathbf{J}_\alpha \mathbf{u}_\alpha + \mathbf{u}_\tau, \qquad (3b)$$

$$\dot{\boldsymbol{\nu}} = \mathbf{u}_\alpha, \qquad (3c)$$

where,

$$\mathbf{S}^{-1} \triangleq \begin{bmatrix} \sec\phi_2 \cos\phi_3 & -\sec\phi_2 \sin\phi_3 & 0 \\ \sin\phi_3 & \cos\phi_3 & 0 \\ -\tan\phi_2 \cos\phi_3 & \tan\phi_2 \sin\phi_3 & 1 \end{bmatrix}.$$

Note that the independent variables in Eqs. (1) and (3) are θ and t, respectively. The two can be related with the help of Kepler's equation.[2]

Spacecraft Configuration

For the spacecraft considered in this paper, the moments of inertia are,

$$\begin{aligned}
\mathbf{J} &= \mathrm{diag}(27.08, 27.08, 37.50) \cdot 10^3 \ \mathrm{kg{\cdot}m^2}, \\
\mathbf{J}_\alpha &= \mathrm{diag}(0.823, 0.823, 0.823) \ \mathrm{kg{\cdot}m^2}.
\end{aligned}$$

The mass of the spacecraft is $m = 4000$kg and it is propelled by six dual-axis thruster forces where the thrusters are placed according to Table 1. From the table, we can see that firing thrusters F_1 and F_4 with equal force in the positive direction creates a force in the direction of the x-axis and firing them with equal force in opposite directions creates a torque about the y-axis.

Constraints

We consider two types of constraints on the system. The first is a constraint on the available thrust, *i.e.* the limits on the dual-axis thrust forces F_i. Let $\mathbf{F}$ be the thrust force vector given by $\mathbf{F} = (F_1, F_2, F_3, F_4, F_5, F_6)$. For all i, F_i is constrained to vary between -0.02 N and 0.02 N, *i.e.*,

$$\|\mathbf{F}\|_\infty \leq 0.02 \ \mathrm{N}. \qquad (4)$$

Thruster	Direction of thrust	Position (m)
F_1	$(1,0,0)$	$(0,0,5)$
F_2	$(0,1,0)$	$(7.5,0,0)$
F_3	$(0,0,1)$	$(0,7.5,0)$
F_4	$(1,0,0)$	$(0,0,-5)$
F_5	$(0,1,0)$	$(-7.5,0,0)$
F_6	$(0,0,1)$	$(0,-7.5,0)$

Table 1. Thruster placements

Because the constraints are on the thrusters but the control algorithm calculates forces and torques, we need to relate one to the other. Let $\mathbf{C}_\theta$ be the rotation matrix from $\mathcal{F}_I$ to $\mathcal{F}_O$. This matrix depends solely on the true anomaly and is given by,

$$\mathbf{C}_\theta = \begin{bmatrix} \cos\theta & \sin\theta & 0 \\ -\sin\theta & \cos\theta & 0 \\ 0 & 0 & 1 \end{bmatrix}.$$

The equation relating the force exerted by the thrusters to the forces and torques exerted by them on the spacecraft is given by,

$$\begin{bmatrix} \mathbf{C}_B \mathbf{C}_\theta^{\mathrm{T}} \mathbf{u}_t \\ \mathbf{u}_\tau \end{bmatrix} = \begin{bmatrix} \mathbf{L}_1 & \mathbf{L}_1 \\ \mathbf{L}_2 & -\mathbf{L}_2 \end{bmatrix} \mathbf{F}, \tag{5}$$

where,

$$\mathbf{L}_1 = \begin{bmatrix} 1 & 0 & 0 \\ 0 & 1 & 0 \\ 0 & 0 & 1 \end{bmatrix}, \ \mathbf{L}_2 = \begin{bmatrix} 0 & 0 & 5 \\ 7.5 & 0 & 0 \\ 0 & 7.5 & 0 \end{bmatrix}.$$

We now assume that $\mathbf{C}_B \approx \mathbf{I}$ and note that such an approximation can be enforced through constraints on attitude error. This approximation and Eq. (5) imply that,

$$\mathbf{F} \approx \begin{bmatrix} \mathbf{C}_\theta \mathbf{L}_1 & \mathbf{C}_\theta \mathbf{L}_1 \\ \mathbf{L}_2 & -\mathbf{L}_2 \end{bmatrix}^{-1} \begin{bmatrix} \mathbf{u}_t \\ \mathbf{u}_\tau \end{bmatrix}, \tag{6}$$

and therefore the constraint on the control inputs is given by,

$$\left\| \begin{bmatrix} \mathbf{C}_\theta \mathbf{L}_1 & \mathbf{C}_\theta \mathbf{L}_1 \\ \mathbf{L}_2 & -\mathbf{L}_2 \end{bmatrix}^{-1} \begin{bmatrix} \mathbf{u}_t \\ \mathbf{u}_\tau \end{bmatrix} \right\|_\infty \leq 0.02. \tag{7}$$

As alluded to above, we are required to keep $\mathbf{C}_B$ close to identity and we can do this by enforcing tight constraints on the attitude error. In the following, we impose a tight constraint on the Euler angles given by,

$$\|\boldsymbol{\phi}\|_\infty \leq 0.03. \tag{8}$$

CONTROL SCHEMES FOR STATION-KEEPING AND MOMENTUM-MANAGEMENT

Common methods of trajectory tracking based on LQ techniques[7,8] do not take into account state and control constraints that subject the controller and plant to limitations. On the other hand, controllers based on MPC are designed to take constraints into account while stabilizing to a desired set-point[9] or tracking a desired reference.[10] In this section, we introduce three MPC methods for tracking a prescribed halo orbit trajectory while satisfying the imposed constraints. Since MPC is related to LQ, we also introduce three related LQR schemes for use in the unconstrained case.

Let $\mathbf{r}(\theta)$ be a vector of coordinates in $\mathbf{F}_O$ that represents a halo orbit solution to Eq. (1) of period T, *i.e.* $\mathbf{r}(\theta) = \mathbf{r}(\theta + nT)$ for any n. Since MPC is applied to discrete-time systems, we choose N points on $r(\theta)$ spaced apart by $\theta_h = \frac{T}{N}$. Let these points be denoted by $\mathbf{r}_k$ so that $\mathbf{r}_k = \mathbf{r}(k\theta_h)$, $k = 0, 1, 2, \ldots, N-1$.

Let $\mathbf{p}_k$ be the 15-dimensional state consisting of discrete samples of $(\boldsymbol{\xi}, \boldsymbol{\xi}', \boldsymbol{\phi}, \boldsymbol{\omega}, \boldsymbol{\nu})$ at time-instant k. Define the tracking error,

$$\mathbf{x}_k = \mathbf{p}_k - \begin{bmatrix} \mathbf{r}_k \\ 0 \end{bmatrix},$$

where 0 represents a 9-dimensional vector of zeros which is our desired set-point for the variables $\boldsymbol{\phi}$, $\boldsymbol{\omega}$, and $\boldsymbol{\nu}$. Define $\mathbf{u}_k$ to be the 9-dimensional discrete-time control input consisting of $(\mathbf{u}_t, \mathbf{u}_\tau, \mathbf{u}_\alpha)$ held constant between samples.

For each $\mathbf{r}_k$, there exists a corresponding $(\mathbf{A}_k, \mathbf{B}_k)$ pair, a local linear mapping from a neighborhood of $(\mathbf{r}_k, 0)$ and $u_k = 0$ to a neighborhood of $(\mathbf{r}_{k+1}, 0)$ that can be obtained by numerical discretization. See the appendix for details.

The methods presented in this paper use the pair $(\mathbf{A}_k, \mathbf{B}_k)$ in order to predict the future trajectory and minimize a penalty function with $\mathbf{x}_k$ and $\mathbf{u}_k$ as parameters, thereby ensuring tracking of the halo orbit and stabilization of the attitude variables. Note that by periodicity, $(\mathbf{A}_{k+nN}, \mathbf{B}_{k+nN}) = (\mathbf{A}_k, \mathbf{B}_k)$ for any integer n.

In what follows, we present three LQ and three MPC schemes for the control of spacecraft station-keeping and momentum-management.

Averaged-in-time LQR (ALQR)

Let $(\mathbf{A}, \mathbf{B}) = \frac{1}{N}\sum_{i=0}^{N-1}(\mathbf{A}_k, \mathbf{B}_k)$ be the averaged dynamics-input matrix pair. We choose symmetric positive-definite cost matrices $\mathbf{Q} \in \mathbb{R}^{15\times 15}$ and $\mathbf{R} \in \mathbb{R}^{9\times 9}$ and solve the following optimization problem,

$$\begin{aligned} &\min_{\{\mathbf{u}_{k+i|k}\}} \frac{1}{2}\sum_{i=0}^{\infty} \mathbf{x}_{k+i|k}^{\mathrm{T}}\mathbf{Q}\mathbf{x}_{k+i|k} + \mathbf{u}_{k+i|k}^{\mathrm{T}}\mathbf{R}\mathbf{u}_{k+i|k}, \\ &\text{sub. to } \mathbf{x}_{k+i+1|k} = \mathbf{A}\mathbf{x}_{k+i|k} + \mathbf{B}\mathbf{u}_{k+i|k}. \end{aligned} \tag{9}$$

The solution to Eq. (9) is a well-known[7] feedback law $\mathbf{u}_{k+i|k} = -\mathbf{K}\mathbf{x}_{k+i|k}$ where,

$$\mathbf{K} = (\mathbf{R} + \mathbf{B}^{\mathrm{T}}\mathbf{P}\mathbf{B})^{-1}\mathbf{B}^{\mathrm{T}}\mathbf{P}\mathbf{A}, \tag{10}$$

and $\mathbf{P}$ is the symmetric positive-definite solution to the discrete-time algebraic Riccati equation,

$$\mathbf{P} = \mathbf{Q} + \mathbf{A}^{\mathrm{T}}\mathbf{P}\mathbf{A} - \mathbf{A}^{\mathrm{T}}\mathbf{P}\mathbf{B}\mathbf{K}. \tag{11}$$

The averaged-in-time control law is,

$$\mathbf{u}_k = -\mathbf{K}\mathbf{x}_k. \tag{12}$$

Fixed-in-time LQR (FLQR)

The parametrization of the halo orbit consists of N states equally spaced apart in true anomaly. We develop a schedule of gains calculated by discretizing Eq. (1) at each time-step and assuming the dynamics-input matrices stay constant for future time. The procedure follows.

We choose symmetric positive-definite cost matrices $\mathbf{Q}_k \in \mathbb{R}^{15\times15}$ and $\mathbf{R}_k \in \mathbb{R}^{9\times9}$, $k = 0, 1, \ldots, N-1$, where $\mathbf{Q}_{k+nN} = \mathbf{Q}_k$ and $\mathbf{R}_{k+nN} = \mathbf{R}_k$ for all n. At each time-step k, we solve the optimization problem,

$$\begin{aligned} &\min_{\{\mathbf{u}_{k+i|k}\}} \frac{1}{2}\sum_{i=0}^{\infty} \mathbf{x}_{k+i|k}^{\mathrm{T}}\mathbf{Q}_k\mathbf{x}_{k+i|k} + \mathbf{u}_{k+i|k}^{\mathrm{T}}\mathbf{R}_k\mathbf{u}_{k+i|k}, \\ &\text{sub. to } \mathbf{x}_{k+i+1|k} = \mathbf{A}_k\mathbf{x}_{k+i|k} + \mathbf{B}_k\mathbf{u}_{k+i|k}, \end{aligned} \tag{13}$$

The solution is given by $\mathbf{u}_{k+i|k} = -\mathbf{K}_k\mathbf{x}_{k+i|k}$, where,

$$\mathbf{K}_k = (\mathbf{R}_k + \mathbf{B}_k^{\mathrm{T}}\mathbf{P}_k\mathbf{B}_k)^{-1}\mathbf{B}_k^{\mathrm{T}}\mathbf{P}_k\mathbf{A}_k, \tag{14}$$

and $\mathbf{P}_k$ is the symmetric positive-definite solution to the discrete-time algebraic Riccati equation,

$$\mathbf{P}_k = \mathbf{Q}_k + \mathbf{A}_k^{\mathrm{T}}\mathbf{P}_k\mathbf{A}_k - \mathbf{A}_k^{\mathrm{T}}\mathbf{P}_k\mathbf{B}_k\mathbf{K}_k. \tag{15}$$

The fixed-in-time control law is,

$$\mathbf{u}_k = -\mathbf{K}_k\mathbf{x}_k. \tag{16}$$

Periodic LQR (PLQR)

Previously, the cost function was minimized assuming that the error dynamics closely adhere to dynamic equations that are time-invariant. However, the dynamics are time-varying and thus we propose a control scheme that utilizes a time-varying model of the error dynamics.

Choose weighting matrices $\mathbf{Q}_k$ and $\mathbf{R}_k$ as above. Solve the optimization problem,

$$\begin{aligned} &\min_{\{\mathbf{u}_{k+i|k}\}} \frac{1}{2}\sum_{i=0}^{\infty} \mathbf{x}_{k+i|k}^{\mathrm{T}}\mathbf{Q}_{k+i}\mathbf{x}_{k+i|k} + \mathbf{u}_{k+i|k}^{\mathrm{T}}\mathbf{R}_{k+i}\mathbf{u}_{k+i|k}, \\ &\text{sub. to } \mathbf{x}_{k+i+1|k} = \mathbf{A}_{k+i}\mathbf{x}_{k+i|k} + \mathbf{B}_{k+i}\mathbf{u}_{k+i|k}. \end{aligned} \tag{17}$$

The solution to Eq. (23) has the form $\mathbf{u}_{k+i|k} = -\mathbf{K}_{k+i}\mathbf{x}_{k+i|k}$ where for all integers i,

$$\mathbf{K}_i = (\mathbf{R}_i + \mathbf{B}_i^{\mathrm{T}}\mathbf{P}_{i+1}\mathbf{B}_i)^{-1}\mathbf{B}_i^{\mathrm{T}}\mathbf{P}_{i+1}\mathbf{A}_i, \tag{18}$$

$$\mathbf{P}_i = \mathbf{Q}_i + \mathbf{A}_i^{\mathrm{T}}\mathbf{P}_{i+1}\mathbf{A}_i - \mathbf{A}_i^{\mathrm{T}}\mathbf{P}_{i+1}\mathbf{B}_i\mathbf{K}_i. \tag{19}$$

Note that due to periodicity, $\mathbf{P}_{i+nN} = \mathbf{P}_i$ and hence $\mathbf{K}_{i+nN} = \mathbf{K}_i$ for all n. To quickly obtain an accurate solution to Eq. (19), we note that Eq. (19) is stable backwards-in-time and use Hewer's method,[7] choosing a symmetric positive-definite initial $\mathbf{P}_0$ and iterating Eq. (19) backwards until we obtain a sequence of N matrices $\mathbf{P}_i$ that has converged. The periodic LQR control law is,

$$\mathbf{u}_k = -\mathbf{K}_k\mathbf{x}_k. \tag{20}$$

The method presented above is the only one to possess guaranteed convergence properties for the linearized time-periodic model. Apart from the degenerate case where $(\mathbf{A}_k, \mathbf{B}_k)$ are constant, it is not guaranteed that $\mathbf{x}_k$ will converge to 0 when using ALQR or FLQR.[11]

Averaged-in-time MPC (AMPC)

Model predictive control (MPC) is a feedback control scheme based on minimizing a quadratic cost subject to pointwise-in-time constraints using a prediction finitely many time-steps into the future.[9,12] At the end of the prediction horizon, MPC imposes a terminal constraint along with a terminal cost to ensure stability. In the following, the constraints are imposed through a set-inclusion constraint. The constraint set is denoted $\mathcal{C} \subset \mathbb{R}^{15} \times \mathbb{R}^9$ and is assumed to be compact and contain 0 in its interior. The terminal constraint set $\mathcal{X}_T \subset \mathbb{R}^{15}$ satisfies the invariance condition that if $x_k \in \mathcal{X}_T$, then $x_{k+1} \in \mathcal{X}_T$ under the application of the control $\mathbf{u}_k = -\mathbf{K}_k \mathbf{x}_k$. For a detailed explanation of the properties and purpose of the terminal set, see Reference 12. The length of the prediction horizon is chosen as N_c, which may not be equal to N.

The AMPC control is obtained by solving the following constrained optimization problem,

$$\begin{aligned}
&\min_{\{\mathbf{u}_{k+i|k}\}} \frac{1}{2}\mathbf{x}_{k+N_c|k}^{\mathrm{T}}\mathbf{P}\mathbf{x}_{k+N_c|k} + \frac{1}{2}\sum_{i=0}^{N_c-1} \mathbf{x}_{k+i|k}^{\mathrm{T}}\mathbf{Q}\mathbf{x}_{k+i|k} + \mathbf{u}_{k+i|k}^{\mathrm{T}}\mathbf{R}\mathbf{u}_{k+i|k}, \\
&\text{sub. to } \mathbf{x}_{k+i+1|k} = \mathbf{A}\mathbf{x}_{k+i|k} + \mathbf{B}\mathbf{u}_{k+i|k}, \\
&\qquad (\mathbf{x}_{k+i|k}, \mathbf{u}_{k+i|k}) \in \mathcal{C}, \\
&\qquad \mathbf{x}_{k+N_c|k} \in \mathcal{X}_T,
\end{aligned} \tag{21}$$

where the terminal cost is obtained using the penalty matrix $\mathbf{P}$ computed in Eq. (15). The control is set to the first element of the sequence resulting from the optimization,

$$\mathbf{u}_k = \mathbf{u}_{k|k}^*. \tag{22}$$

The values above have already been introduced in the section describing the ALQR scheme. If the inequality constraints are not active, the control coincides with the output of the ALQR.

Fixed-in-time MPC (FMPC)

The following MPC scheme uses instantaneously fixed dynamics for prediction as opposed to the averaged dynamics used in the previous section. The control is obtained by solving the following constrained optimization problem,

$$\begin{aligned}
&\min_{\{\mathbf{u}_{k+i|k}\}} \frac{1}{2}\mathbf{x}_{k+N_c|k}^{\mathrm{T}}\mathbf{P}_k\mathbf{x}_{k+N_c|k} + \frac{1}{2}\sum_{i=0}^{N_c-1} \mathbf{x}_{k+i|k}^{\mathrm{T}}\mathbf{Q}_k\mathbf{x}_{k+i|k} + \mathbf{u}_{k+i|k}^{\mathrm{T}}\mathbf{R}_k\mathbf{u}_{k+i|k}, \\
&\text{sub. to } \mathbf{x}_{k+i+1|k} = \mathbf{A}_k\mathbf{x}_{k+i|k} + \mathbf{B}_k\mathbf{u}_{k+i|k}, \\
&\qquad (\mathbf{x}_{k+i|k}, \mathbf{u}_{k+i|k}) \in \mathcal{C}, \\
&\qquad \mathbf{x}_{k+N_c|k} \in \mathcal{X}_T,
\end{aligned} \tag{23}$$

and the control is set to the first element of the sequence resulting from the optimization,

$$\mathbf{u}_k = \mathbf{u}_{k|k}^*. \tag{24}$$

If the inequality constraints are not active, the control coincides with the output of the FLQR.

Periodic MPC (PMPC)

We consider here the MPC scheme for time-periodic systems.[13] In it, a quadratic cost function is minimized subject to constraints and time-varying dynamics. PMPC is based on a solution to the following constrained optimization problem,

$$\begin{aligned}
&\min_{\{\mathbf{u}_{k+i|k}\}} \frac{1}{2}\mathbf{x}_{k+N_c|k}^{\mathrm{T}}\mathbf{P}_{k+N_c}\mathbf{x}_{k+N_c|k} + \frac{1}{2}\sum_{i=0}^{N_c-1}\mathbf{x}_{k+i|k}^{\mathrm{T}}\mathbf{Q}_{k+i}\mathbf{x}_{k+i|k} + \mathbf{u}_{k+i|k}^{\mathrm{T}}\mathbf{R}_{k+i}\mathbf{u}_{k+i|k}, \\
&\text{sub. to } \mathbf{x}_{k+i+1|k} = \mathbf{A}_{k+i}\mathbf{x}_{k+i|k} + \mathbf{B}_{k+i}\mathbf{u}_{k+i|k}, \\
&\qquad (\mathbf{x}_{k+i|k}, \mathbf{u}_{k+i|k}) \in \mathcal{C}, \\
&\qquad \mathbf{x}_{k+N_c|k} \in \mathcal{X}_T,
\end{aligned} \tag{25}$$

where $\mathbf{P}_k$ is the solution to the periodic difference Riccati equation (19). The control is set to the first element of the sequence solving Eq. (25).

$$\mathbf{u}_k = \mathbf{u}_{k|k}^*. \tag{26}$$

If the inequality constraints are not active, the control coincides with the output of the PLQR.

As with PLQR, PMPC is the only MPC scheme to possess guaranteed theoretical properties for the linearized time-periodic model as explained in Reference 13. Namely, if we start close enough so that a solution to Eq. (25) exists, then we are guaranteed constraint enforcement and convergence to the desired set-point, *i.e.* $\mathbf{x}_k$ tends to the origin and the constraints are not violated. Furthermore, by properly designing the terminal constraint, stability guarantees in determined domain of attractions are also obtained.

NUMERICAL RESULTS

Simulation Parameters

In our simulations, we consider the halo orbit about the Earth-Moon Lagrangian point L2. Ignoring the gravitational effects of any other celestial bodies, we begin by assuming the Earth-Moon orbit is circular, *i.e.* $e = 0$, and the distance between the two bodies is 384,362 km.

We compute three different orbits for comparing our tracking schemes using numerical methods described in detail in Reference 3. The three orbits are (i) the smallest possible orbit – equilibrium at L2, (ii) a small orbit, whose diameter is chosen such that the spacecraft barely establishes a line of sight with the Earth, and (iii) a large orbit, whose diameter is chosen to be much larger. All orbits are restricted to the x-y plane. This is chosen because $z \equiv 0$ is a solution to the 3-body equations of motion and motion in the z-axis is not required to compute a halo orbit. The orbits are plotted in Figure 2.

In all subsequent simulations, $\mathbf{Q}_k \equiv \mathbf{Q}$ and $\mathbf{R}_k \equiv \mathbf{R}$ are kept constant and,

$$\mathbf{Q} = \begin{bmatrix} 10^6\mathbf{I}_3 & 0 \\ 0 & \mathbf{I}_{12} \end{bmatrix}, \ \mathbf{R} = 10^6\mathbf{I}_9. \tag{27}$$

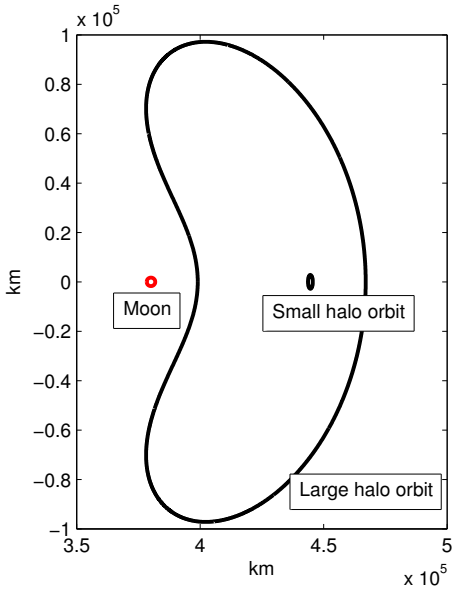

Figure 2. Plot of the small and large halo orbits considered in this paper

Determining the Length of the Discretization Time-Step

Our first numerical simulation solely considers station-keeping on the large halo orbit and does not consider constraints or attitude control; its purpose is to determine the desired true anomaly-step length. A smaller true anomaly-step length is desired because it better approximates a smooth control response and may lower the control cost. However, more steps are needed if the prediction horizon is to be kept constant and therefore smaller steps result in a larger computational burden for the MPC schemes presented above; it is possible to lower the computational burden by scaling the prediction horizon with the true anomaly-step, but this results in a myopic prediction and may lead to a smaller region of attraction.

The initial condition is taken to be a 100 km error in the x-direction with all other parameters matching the halo orbit at time-instant $k = 0$, *i.e.* $[\mathbf{x}_0]_1 = 100$ km and $[\mathbf{x}_0]_i = 0$ for all $i \neq 1$. Because the orbit of the primaries is circular, the relationship between scaled time-step t_h and the step in true anomaly θ_h stays constant, *i.e.* $t_h = \theta_h$. We compare three different choices of N corresponding to time-steps of approximately one minute, one hour, and one day. Due to the fact that this is an unconstrained problem, we consider only the ALQR, FLQR, and PLQR schemes introduced above, tabulating the total $\Delta v_{tot} = \sum_k \theta_h(|[\mathbf{u}_k]_1|, |[\mathbf{u}_k]_2|)$ in Table 2.

The results are consistent for different choices of initial conditions. The PLQR achieves the lowest Δv_{tot} and there is no large difference in Δv_{tot} when choosing between a true anomaly-step corresponding to 6 minutes and 1 hour, as compared to the case of a true anomaly-step corresponding to a day. Hence we fix the true anomaly-step at 0.534° and retain the PLQR and PMPC schemes for further investigation.

Run No.	i	ii	iii
N	4294	430	18
t_h	6.00min	1.00hr	0.95day
θ_h	0.0534°	0.534°	13.5°
ALQR Δv_{tot} (m/s)	(5.20,7.55)	(5.31,7.72)	(9.20, 9.47)
FLQR Δv_{tot} (m/s)	(8.51,5.60)	(9.20,6.20)	DNC
PLQR Δv_{tot} (m/s)	(3.77,5.83)	(4.01,5.85)	(4.70,6.89)

Table 2. Impact of discretization choices on Δv (DNC: "did not converge")

Station-Keeping Using PLQR

We next perform station-keeping simulations for the most advanced LQR-based scheme, the PLQR scheme. The initial condition is changed to $[\mathbf{x}_0]_1 = 10^3$km, $[\mathbf{x}_0]_6 = 10^3$km/orbit with all other initial conditions held constant at 0. A large initial condition is chosen in order to illustrate the capability of the schemes. As previously stated, we consider three different orbits: no orbit (stabilization to L2), a small orbit, and a large orbit. We plot the responses in the no orbit case in Figures 4 and 5. Note that in this case, the controller stabilizes the spacecraft to the L2 point and reduces to ordinary LQR control. The rest of the results are plotted in Figures 6-11.

Combined Station-Keeping and Momentum-Management

In this simulation we consider the full problem with both translational and attitude control. Applying the PMPC scheme to the system subject to the constraints described previously, we simulate the closed-loop response from an initial condition of $[\mathbf{x}_0]_1 = 40$ km, $[\mathbf{x}_0]_2 = -40$ km and a reaction wheel spin of 100 radians per second about the z-axis, *i.e.* $[\mathbf{x}_0]_{15} = 100$ rad/s; all other initial conditions are set to 0. The results are presented in Figures 12-16.

Figure 12 shows the translational force responses $F_x = mu_x$ and $F_y = mu_y$ as well as the torque response in the z-axis. Figure 13 shows Δv as a function of time. Figure 14 shows the eigenaxis error about the z-axis along with the constraint of Eq. (8). As we can see, the constraint is enforced pointwise-in-time but not between points. This is because MPC is a discrete-time control method that can only enforce constraints for specific points in time. Figures 15 and 16 show the radial velocity of the spacecraft about the z-axis and the z-axis reaction wheel velocity. Finally, Figure 17 shows the constraint adherence corresponding to the constraint of Eq. (4). Close to the beginning of the simulation, the thrust constraints are violated by a very small amount and this is due to the approximation $\mathbf{C}_B \approx \mathbf{I}$ in Eq. (6). To avoid such a constraint violation in application, the force vector $\mathbf{F}$ could be computed by assuming $\mathbf{C}_B = \mathbf{I}$.

An interesting observation is that MPC is able to balance the thrust used in delivering the requested translational force and the requested torques. At first, the thruster F_5 provides positive thrust in order to provide torque and stabilize the attitude while enforcing the pointing constraint of Eq. (8); it then provides a negative thrust at the constraint boundary in order to stabilize the tracking error.

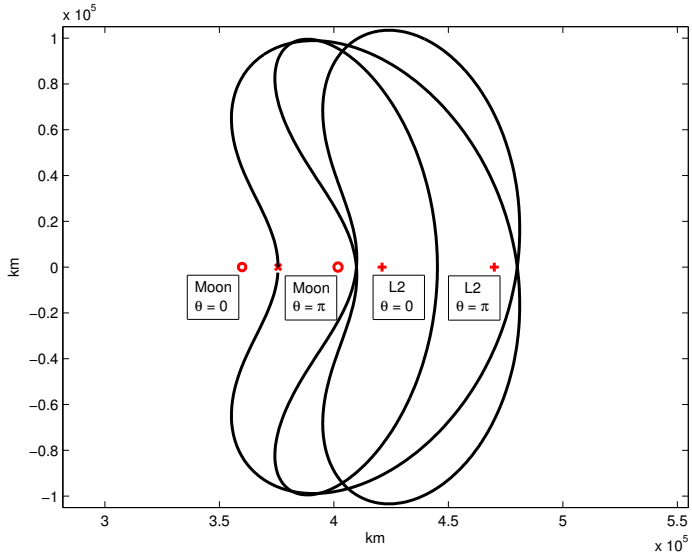

Figure 3. Halo orbit in the Earth-Moon system with eccentricity $e = 0.055$ and period 4π; $\circ$ and $+$ indicate the locations of the Moon and L2, respectively, at $\theta = 0$ and π and $\times$ indicates the initial condition of the trajectory at $\theta = 0$

Elliptical Orbits

For the final simulation, we set values that are representative of the Earth-Moon scenario. The eccentricity is set to a non-zero value of $e = 0.055$ and the semi-latus rectum to 384,362 km.

In the elliptical case, the halo orbit is closed if the period of the trajectory is equal to $T = k\pi$ for some integer k. In our simulation, we choose the value of the period to be $T = 4\pi$ because this results in a large orbit. The orbit is plotted in Figure 3. The results are plotted in Figures 18 and 19. Because attitude is set to rest, unlike the results of Figure 17 the thrust trajectory in Figure 19 immediately reaches force limits at the beginning of the simulation.

CONCLUSION

This paper considered the application of Linear Quadratic Regulator and Model Predictive Control techniques to the problem of tracking the Earth-Moon halo orbit about L2 and simultaneous attitude control.

Several numerical investigations were reported. Based on the simulations, the periodic MPC was shown to result in the lowest fuel consumption. The viability of periodic MPC was also shown for simultaneous station-keeping and momentum-management. The final numerical simulation showed a spacecraft closed-loop controlled by periodic MPC successfully tracking an elliptical halo orbit while enforcing constraints.

ACKNOWLEDGMENT

The authors gratefully acknowledge Dr. Stefano Campagnola of JAXA for a technical discussion on how to compute a halo orbit in the case of non-zero eccentricity.

REFERENCES

[1] B. Wie, *Space Vehicle Dynamics and Control*. Reston, VA: AIAA, 2nd ed., 2008.

[2] A. de Ruiter, C. J. Damaren, and J. R. Forbes, *Spacecraft Dynamics and Control: An Introduction*. West Sussex, UK: Wiley, 2013.

[3] W. S. Koon, M. W. Lo, J. E. Marsden, and S. D. Ross, *Dynamical Systems, the Three-Body Problem and Space Mission Design*. Marsden Books, 2011.

[4] R. W. Farquhar, "Lunar communications with libration-point satellites," *Journal of Spacecraft and Rockets*, Vol. 4, No. 10, 1967, pp. 1383–1384.

[5] S. Campagnola, *New Techniques in Astrodynamics for Moon Systems Exploration*. Dissertation, University of Southern California, 2010.

[6] A. Weiss, I. Kolmanovsky, D. S. Bernstein, and A. Sanyal, "Inertia-free spacecraft attitude control using reactions wheels," *J. of Guidance, Control, and Dynamics*, Vol. 36, No. 5, 2013, pp. 1425–1439.

[7] R. F. Stengel, *Optimal Control and Estimation*. Mineola, NY: Dover, 2nd ed., 1994.

[8] M. Nazari, W. Anthony, and E. A. Butcher, "Continuous Thrust Stationkeeping in Earth-Moon L_1 Halo Orbits Based on LQR control and Floquet Theory," *AIAA/AAS Astrodynamics Specialist Conf.*, AIAA 2014-4140.

[9] D. Q. Mayne, J. B. Rawlings, C. V. Rao, and P. O. M. Scokaert, "Constrained model predictive control: Stability and optimality," *Automatica*, Vol. 36, No. 6, 2000, pp. 789–814.

[10] D. Limon, I. Alvarado, T. Alamo, and E. F. Camacho, "MPC for tracking piecewise constant references for constrained linear systems," *Automatica*, Vol. 44, No. 9, 2008, pp. 2382–2387.

[11] H. K. Khalil, *Nonlinear Systems*. Upper Saddle River, NJ: Prentice Hall, 3rd ed., 2002.

[12] G. C. Goodwin, J. A. D. Doná, and M. M. Seron, *Constrained Control and Estimation: An Optimisation Approach*. London: Springer-Verlag, 2005.

[13] R. Gondhalekar and C. N. Jones, "MPC of constrained discrete-time linear periodic systems – A framework for asynchronous control: Strong feasibility, stability and optimality via periodic invariance," *Automatica*, Vol. 47, No. 2, 2011, pp. 326–333.

APPENDIX: NUMERICAL DISCRETIZATION ALONG SOLUTION TRAJECTORIES

Consider an n-dimensional dynamical system described by,

$$\dot{\mathbf{x}}(t) = f(t, \mathbf{x}(t)).$$

Let $\mathbf{r}(t)$ denote a solution. We wish to compute the discrete-time update for perturbations of $\mathbf{r}(t)$, *i.e.* given a time t_h and a perturbed state $\tilde{\mathbf{r}}(t) = \mathbf{r}(t) + \delta\mathbf{r}(t)$, we wish to find a local linear map $\mathbf{A}(t)$ such that $\tilde{\mathbf{r}}(t + t_h) - \mathbf{r}(t + t_h) \approx A(t)\delta\mathbf{r}(t)$.

To compute $A(t)$ numerically, let $\mathbf{e}_i$ be the elementary basis vector where the i-th element of $\mathbf{e}_i$ is equal to 1 and let $\varepsilon > 0$ be a small parameter. Propagate $\mathbf{r}(t) + \varepsilon\mathbf{e}_i$ and $\mathbf{r}(t) - \varepsilon\mathbf{e}_i$ from t to $t + t_h$ numerically and refer to the solutions at time $t + t_h$ as $\tilde{\mathbf{r}}_i^+$ and $\tilde{\mathbf{r}}_i^-$, respectively. Then, we can approximate the i-th column of $A(t)$ by the center difference formula,

$$\frac{\tilde{\mathbf{r}}_i^+ - \tilde{\mathbf{r}}_i^-}{2\varepsilon}.$$

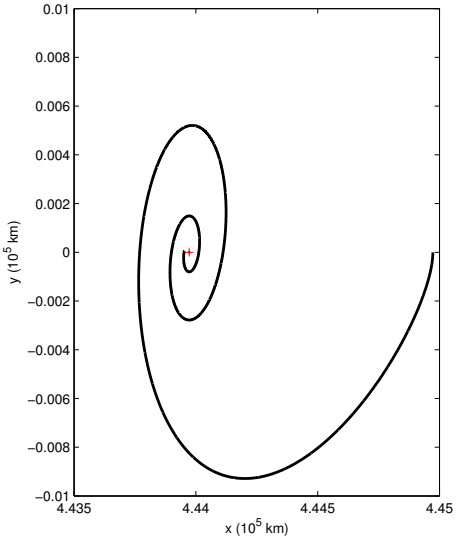

Figure 4. Results of PLQR simulation for no orbit: Orbit trajectory

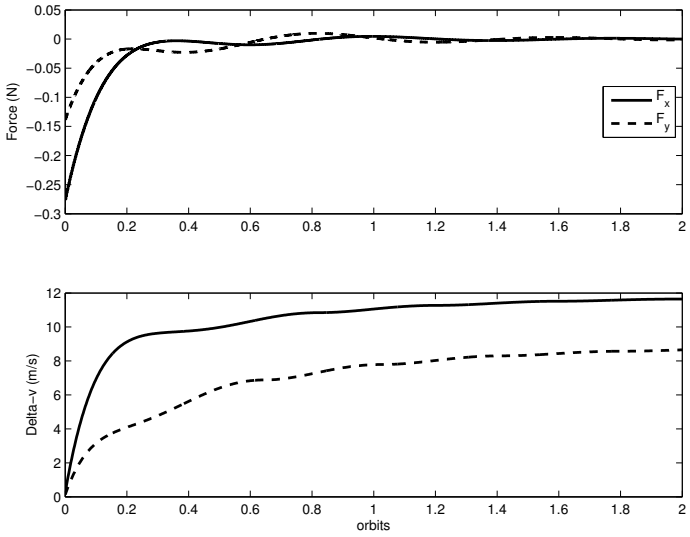

Figure 5. Results of PLQR simulation for no orbit: Time history of $\mathbf{F}_k$ and $\Delta\mathbf{v}_k$

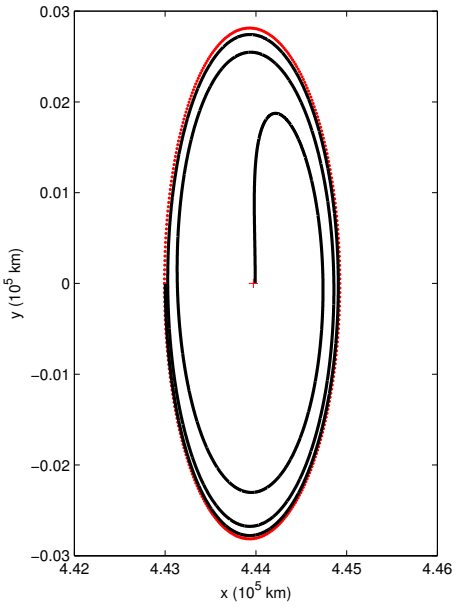

Figure 6. Results of PLQR simulation for small orbit: Orbit trajectory

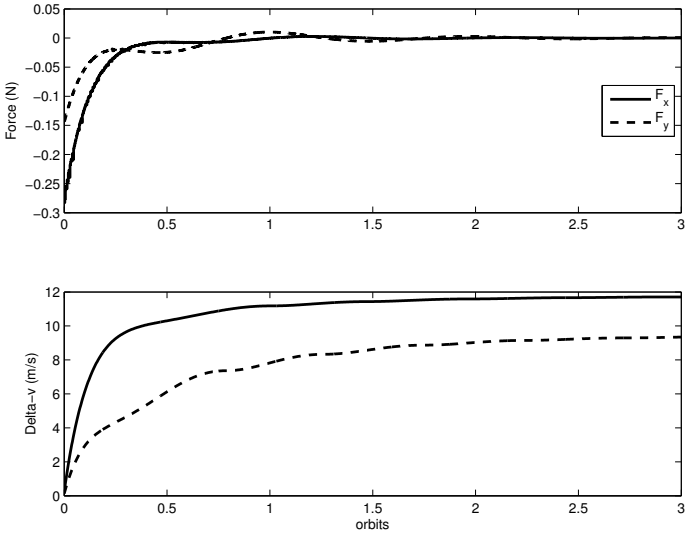

Figure 7. Results of PLQR simulation for small orbit: Time history of $\mathbf{F}_k$ and $\Delta\mathbf{v}_k$

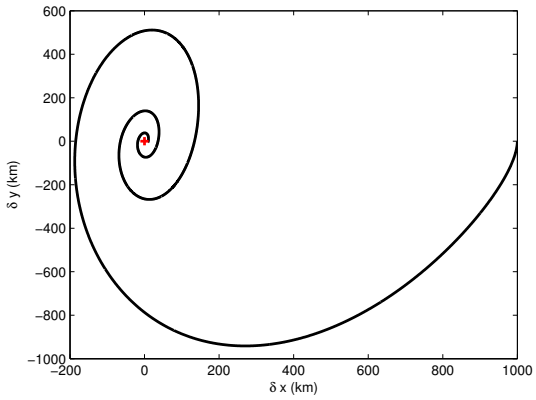

Figure 8. Results of PLQR simulation for small orbit: Error trajectory on x-y plane

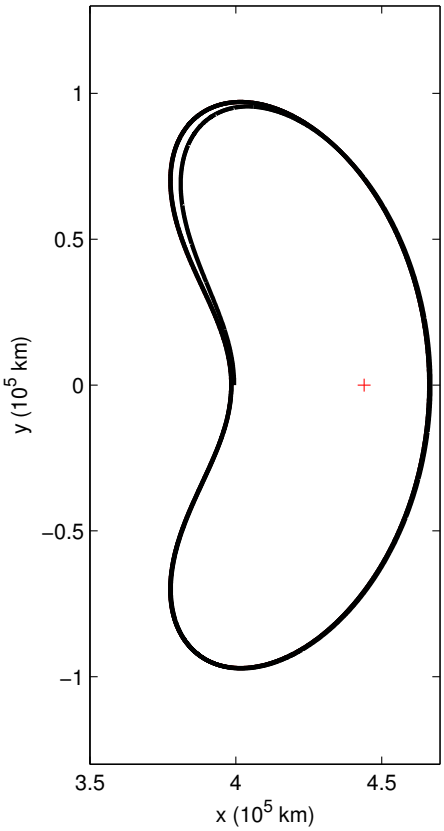

Figure 9. Results of PLQR simulation for large orbit: Orbit trajectory

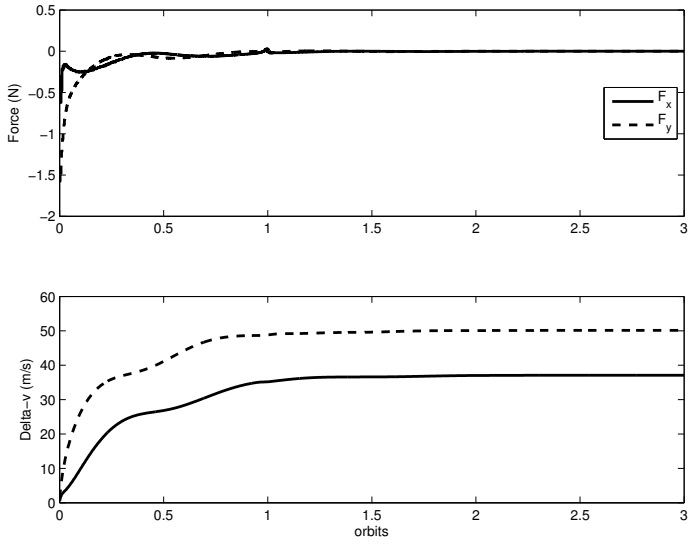

Figure 10. Results of PLQR simulation for large orbit: Time history of $\mathbf{F}_k$ and $\Delta\mathbf{v}_k$

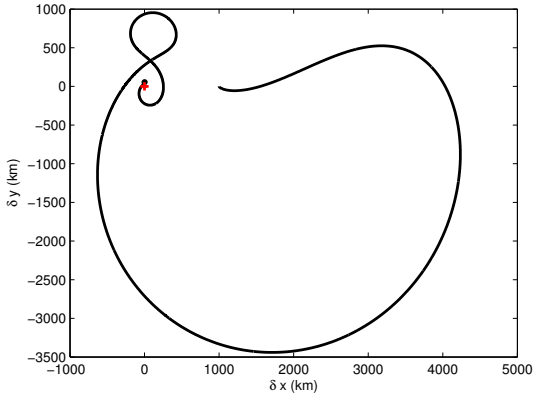

Figure 11. Results of PLQR simulation for large orbit: Error trajectory on x-y plane

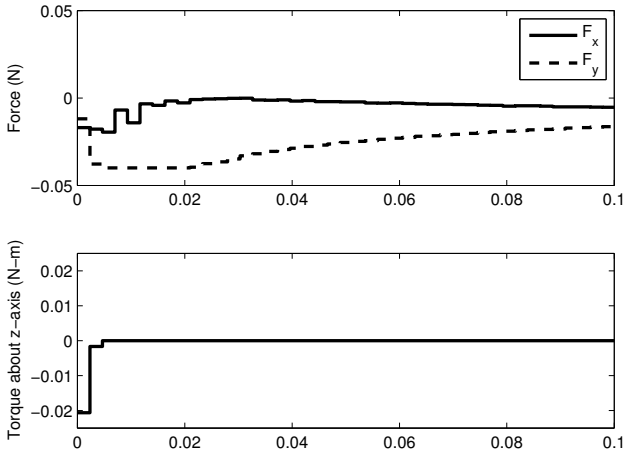

Figure 12. Results of PMPC simulation for large orbit: Required forces and torques

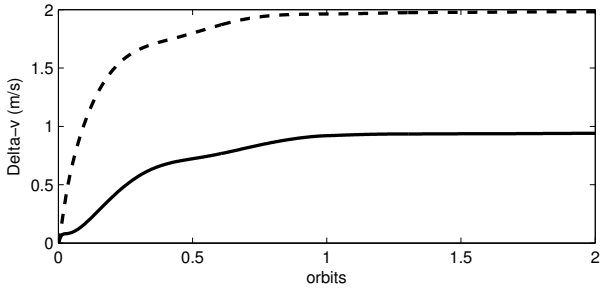

Figure 13. Results of PMPC simulation for large orbit: Δv

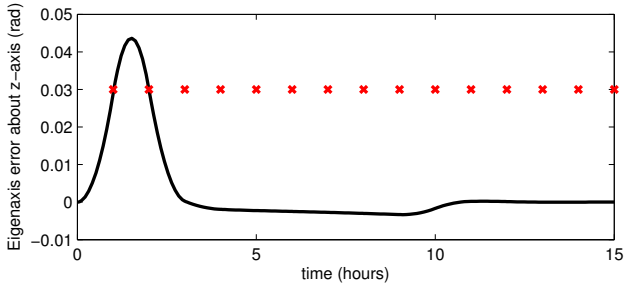

Figure 14. Results of PMPC simulation for large orbit: Pointing error on z-axis. The pointwise-in-time constraints are plotted as dots.

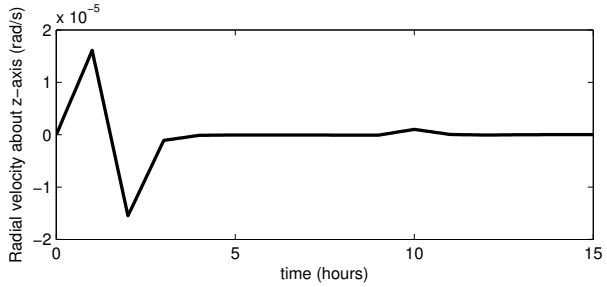

Figure 15. Results of PMPC simulation for large orbit: Radial velocity on z-axis

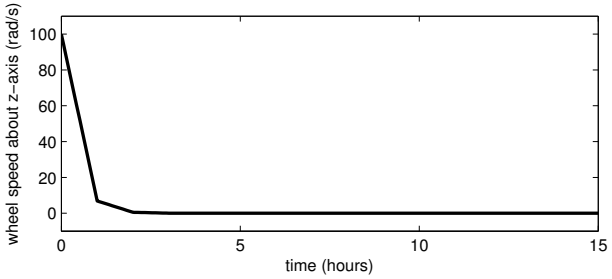

Figure 16. Results of PMPC simulation for large orbit: z-axis reaction wheel velocity

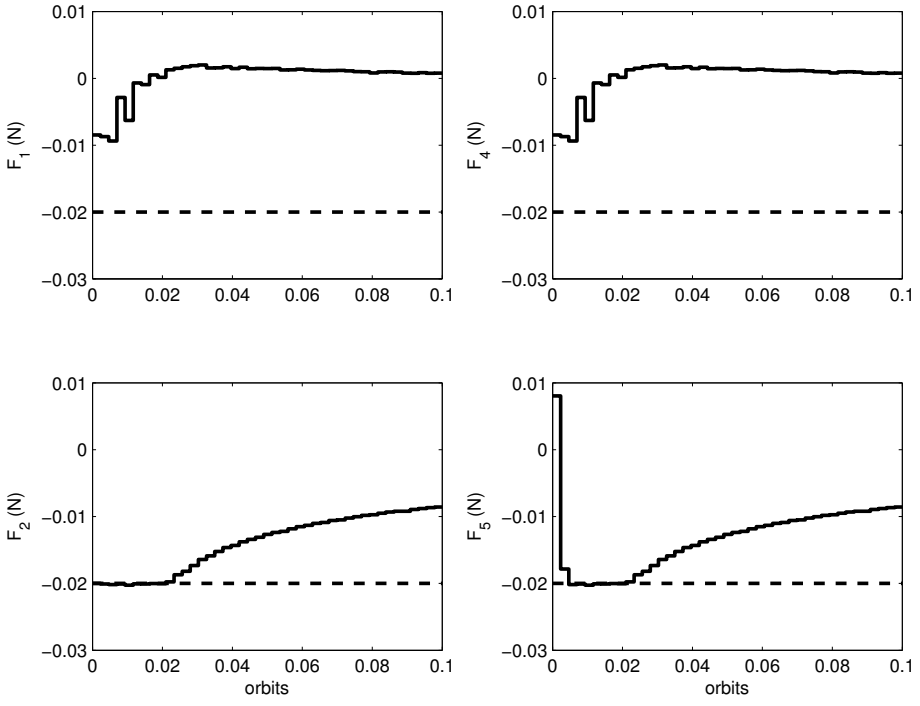

Figure 17. Results of PMPC simulation for large orbit: Thrust force from the dual-axis thrusters placed on the x- and y-axes. The constraints are given by the dashed line.

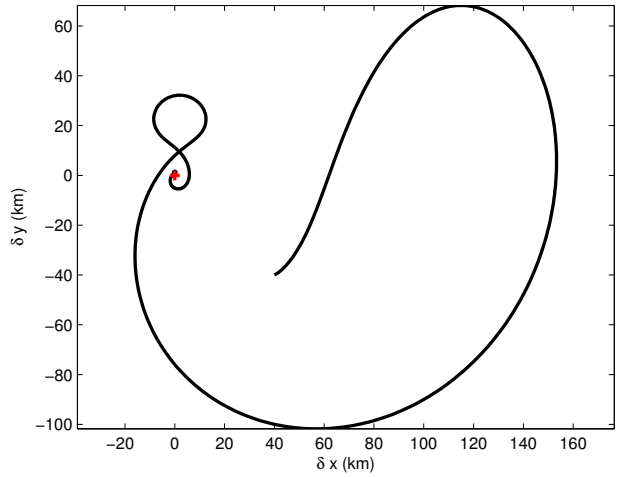

Figure 18. Results of PMPC simulation for eccentric orbit:Error trajectory on x-y plane

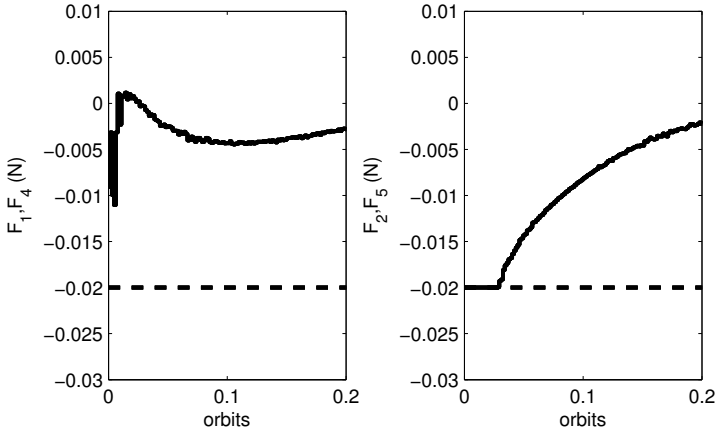

Figure 19. Results of PMPC simulation for eccentric orbit: Thrust force from the dual-axis thrusters placed on the x- and y-axes. The constraints are given by the dashed line.